Nonlinear statistics of daily temperature fluctuations reproduced in a laboratory experiment

Balázs Gyüre,[1] Imre Bartos,[2] and Imre M. Jánosi[1,2,*]
[1]*von Kármán Laboratory for Environmental Flows, Loránd Eötvös University, P.O. Box 32, H-1518 Budapest, Hungary*
[2]*Department of Physics of Complex Systems, Loránd Eötvös University, P.O. Box 32, H-1518 Budapest, Hungary*
(Received 11 September 2006; published 27 September 2007)

The near-global statistics of daily mean temperature changes reveals a robust asymmetry. Warming steps have significantly higher frequency and lower average magnitude than those of cooling steps for most weather stations. This is a markedly nonlinear feature: Fourier surrogate time series exhibit completely symmetric increment statistics. The obtained geographic distribution of asymmetry parameters suggested an experimental test in a classical rotating tank setup. Temperature measurements in the dynamical regime of geostrophic turbulence reproduce quantitatively the strong asymmetry and spatial dependence of field observations. The statistics might be relevant in other systems of nonequilibrium steady states.

DOI: 10.1103/PhysRevE.76.037301 PACS number(s): 47.52.+j, 92.60.−e, 05.45.Jn, 92.10.Ei

In the late 1950s, the discipline of geophysical fluid dynamics emerged from relatively simple mathematical and laboratory models unifying atmospheric and oceanic dynamics. Perfect hydrodynamic similarity, where all the appropriate nondimensional parameters are precisely equal for geophysically relevant scales and "miniaturized" experiments, is not possible [1]. Therefore, a quantitative agreement between field observations and laboratory measurements is exceptional, even if such experiments have continuously been facilitating a better understanding of complex geophysical flows. Here we report on temperature measurements in a classical experimental setup, where a markedly nonlinear feature of daily terrestrial weather records is robustly reproduced.

In a recent work [2], we analyzed the statistical properties of surface temperature records from the Global Daily Climatological Network (GDCN) data bank collected by the NOAA National Climatic Data Center's Climate Analysis Branch [3]. Here we concentrate on the global statistics of mean temperature differences between consecutive days for records longer than 5 years (13 208 stations). A surprisingly simple test revealed a peculiar characteristic summarized in Fig. 1. We observed that the number of warming steps, N_w, is significantly different from the number of cooling steps, N_c, at almost every geographic locations, irrespectively of the length of the record [Fig. 1(a)]. Furthermore, the average magnitude of warming steps $\langle \Delta T_w \rangle$ differs also from the average magnitude of cooling steps $\langle \Delta T_c \rangle$ for most stations [Fig. 1(b)]. Strict stationarity requires a simple inverse relationship between the ratios N_w/N_c and $\langle \Delta T_w \rangle / \langle \Delta T_c \rangle$ for a given record, and we will show that both meteorological and experimental data obey this condition.

Next, we would like to emphasize that the observed asymmetries are signatures of the inherent nonlinear nature of atmospheric circulation. This is verified by implementing the iterative Fourier surrogate time series procedure by Schreiber and Schmitz [4], which destroys higher-order (nonlinear) correlations in a signal by keeping two-point correlations and (usually not entirely Gaussian) amplitude distributions intact. Surrogate temperature data exhibit full symmetry: both ratios drop around 1.00, and statistical fluctuations (mostly due to finite record length) are reflected only to the third digit.

The geographic distribution of step-number or step-size ratios reveals a relatively simple pattern on the northern hemisphere (where the GDCN spatial coverage is much better), illustrated in Fig. 1(c). Although local circumstances (topography, land-use, distance from oceans, etc.) certainly influence weather and climate, the global pattern reflects a smooth overall latitude dependence: the larger the distance from the Horse latitude (~30 °N), the smaller the step number ratio N_w/N_c. Such an uncomplicated behavior suggests that the origin should be linked with the most essential determining factors of atmospheric dynamics: differential heating and rotation.

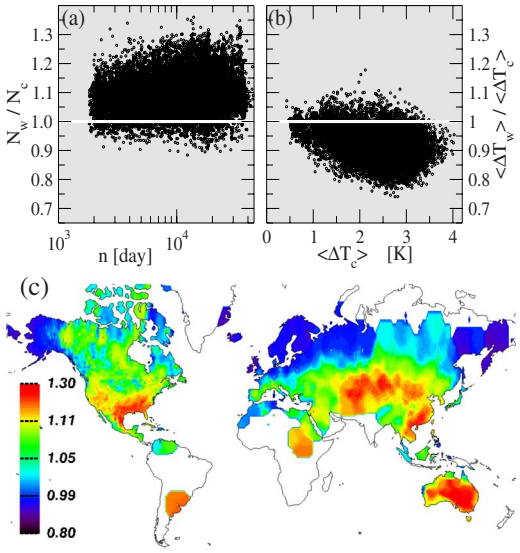

FIG. 1. (Color online) Statistics of daily mean temperature changes for 13 208 weather stations. (a) Number of warming steps, N_w, over the number of cooling steps, N_c, as a function of record length n (the horizontal scale is logarithmic). (b) Average warming step $\langle \Delta T_w \rangle$ over average cooling step $\langle \Delta T_c \rangle$ as a function of the latter for each station. (c) Geographic distribution of the step number ratio shown in (a) (the color scale is nonlinear) [2].

*janosi@lecso.elte.hu

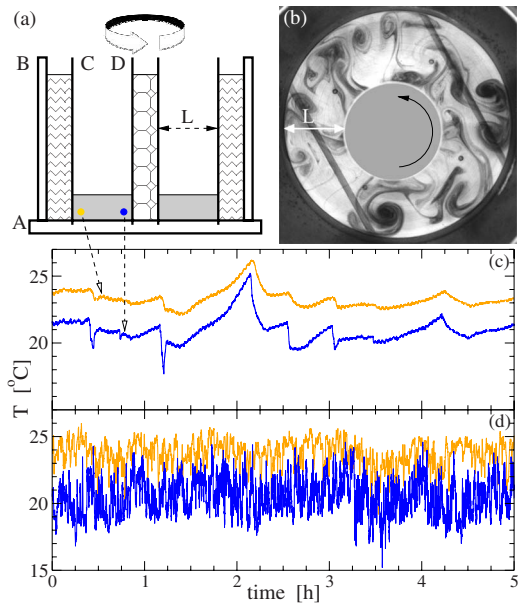

FIG. 2. (Color online) (a) Experimental setup. *A*: Plexiglas bottom plate. *B*: outermost glass cylinder of radius 20.3 cm. *C*: middle copper cylinder of radius 15.0 cm. *D*: inner copper cylinder of radius 4.5 cm. (b) Dye visualization of typical flow patterns in the working fluid of height 4.0 cm (the two slanted stripes are parts of the bottom plate). (c) Example time series recorded in a nonrotating convection experiment with a sampling rate of 3 s. The location of the probes is indicated in (a) by colored circles: distance from the sidewall is 8 mm, height from the bottom is 3 mm in both cases. The warm boundary temperature $T_{w0}=35$ °C; black triangles indicate when ice was refilled in the middle cylinder. (d) The same as (c) rotated with $\Omega=2.73$ s^{-1}.

The classical laboratory model for the midlatitude large-scale flow phenomena is a differentially heated rotating annulus invented by Fultz *et al.* [5,6] and Hide and co-workers [7,8]. The setup, depicted in Fig. 2(a), consists of three concentric cylinders placed on a rotating table. The central container is cooled, the outermost one is heated, and the working fluid in the middle is usually water or solution of glycerol of various viscosities. Besides the traditional dye visualization methods [Fig. 2(b)], arrays of temperature probes [9–13] and modern tools, such as the laser Doppler velocimetry [14] or thermographic cameras [15], are used to collect quantitative information about the flow field. The main control parameters are the rotation rate and imposed temperature difference in a dish of fixed geometry. These are usually expressed by two nondimensional ratios called in recent papers the "Taylor number" and "thermal Rossby number"; however, we do not adopt them here because of the problematic relationship between laboratory and possible atmospheric values. Systematic explorations of the parameter space identified axisymmetric flow fields, steady and vacillating waves, and irregular patterns (geostrophic turbulence [16]); for a review see [17].

We performed temperature measurements in the rotating annulus sketched in Fig. 2(a). Angular velocities in the range $\Omega=1.88-4.71$ s^{-1} at two temperature gradients were imposed: $T_{w0}=35.0\pm0.1$ °C and 40.0 ± 0.1 °C outside, melting ice ($T_{c0}\approx4$ °C) inside. Two corotating Ni-NiCr thermocouples fixed at the end of thin wires (of diameter 0.5 mm) were sampled at a rate of $\Delta t=3.0$ s, which is approximately one sample per revolution (in analogy with the meteorological records). The height of the sensors was fixed at 3 mm from the bottom; the radial positions were changed in the experiments running 5–6 h each. In the nonrotating control experiments we checked the presence of simple radial convection, and measured the typical flow speeds between 0.5 and 1.0 mm/s.

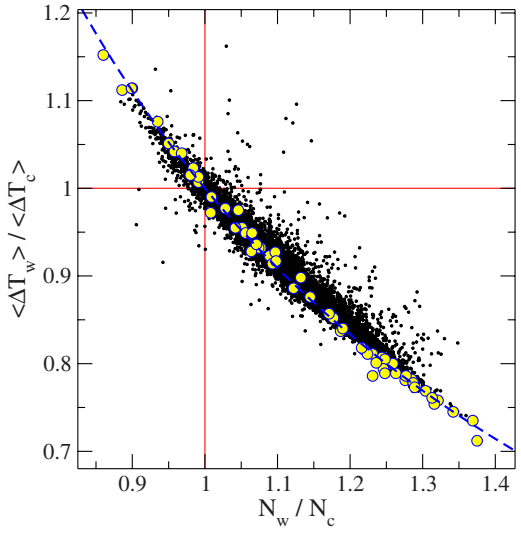

FIG. 3. (Color online) Correlation plot between step number ratio and average step size ratio for temperature changes. Black dots: terrestrial weather stations. Colored circles: laboratory experiments. Dashed line indicates the perfect stationarity condition.

The parameter range we implemented is deeply in the dynamical regime of irregular wave patterns, similarly to the midlatitude atmosphere. Note that the thermal boundary condition was nonstationary inside due to the cyclically varying amount of ice. This is a technical limitation of our setup; however, the midlatitude atmosphere is also not constrained to fixed boundary temperatures. The main effect of rotation is demonstrated by comparing the signals in Fig. 2(c) and 2(d). The large fluctuations indicate strong cyclonic and anticyclonic vortical activity with irregular transits of cold and warm "fronts" at both locations. (Note that the resulting temporal fluctuations have a much shorter time scale than the global temperature control.) It is widely accepted that the dynamics driven by the so-called baroclinic instability reflects the most essential features of midlatitude atmospheric flow (see, e.g., [18,19]).

We evaluated the experimental temperature records in the same way as the meteorological data. We found the same robust asymmetries in the statistics of temperature changes; the results are shown in Fig. 3. The prominent data collapse onto the curve of strict stationarity in Fig. 3 is somewhat surprising for the meteorological data, which means that systematic baseline drifts (urbanization, changing land use, global warming, etc.) are hardly visible in the records.

Alike to the GDCN data, the surrogate time series algorithm [4] results in fully symmetric signals again. Here we

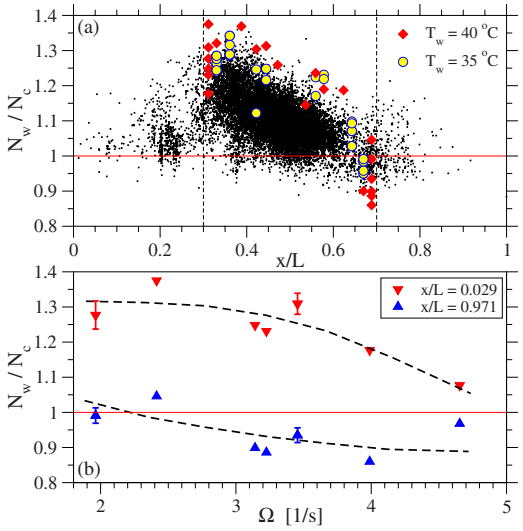

FIG. 4. (Color online) (a) Step number ratio for temperature changes as a function of nondimensional distance from the warm boundary. Black dots: meteorological records. Color symbols: experiments for two control temperatures. Dashed lines indicate the horizontal contraction of the experimental data resulting in approximately the same slope as the meteorological observations. (b) Step number ratio for two fixed locations close to the boundaries as a function of angular velocity Ω, at T_{w0}=40 °C. Dashed lines are only a guide for the eye.

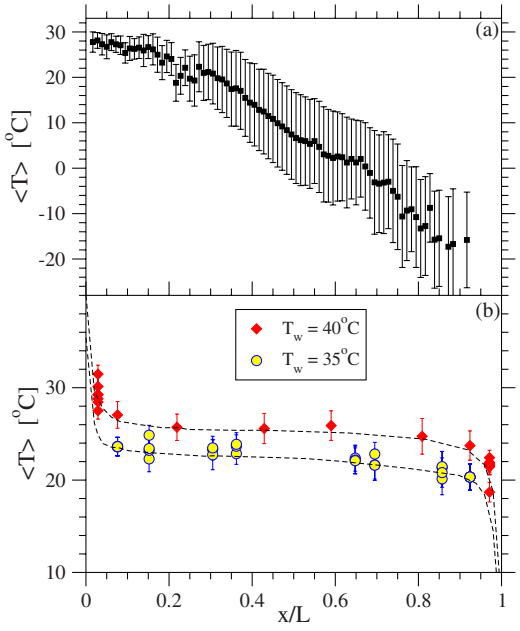

FIG. 5. (Color online) Average temperature profiles as a function of nondimensional distance from the warm boundary. (a) Zonal average for the meteorological records. Error bars represent one standard deviation; seasonality is included. x/L is given by the latitude normalized by $\pi/2$. (b) Profiles in the rotating tank for two control temperatures.

shortly note that all standard procedures [20] failed to detect low-dimensional chaos in both the meteorological and experimental records. This is in agreement with earlier results [21] and expectations in the dynamical regime of geostrophic turbulence. On the other hand, test series generated by baker, Hénon, and Ikeda maps or by the Lorenz equations (variable z) in the fully developed chaotic parameter range [22] exhibit also similarly asymmetric increment distributions, which entirely disappear in the surrogate data.

What determines the extent of asymmetry in an individual time series? The map of Fig. 1(c) suggests the latitude as a primary variable for the meteorological observations, complicated by other factors. Indeed, when the step number ratio is plotted for each station as a function of the nondimensional distance from the equator [Fig. 4(a), black dots], the distribution exhibits a rather smeared structure. The nonmonotonous behavior with a local maximum at around ~30° latitude ($x/L \approx 0.33$) might be related to the cellular organization of the atmospheric circulation—namely, to the descending branch of the Hadley cell [23]. In spite of the large scatter, the main tendency is clearly the same as in the map in Fig. 1(c). This tendency of smaller increment asymmetries at larger distances from the warm boundary is reproduced in the experiments, too [Fig. 4(a), color symbols]. However, an attempt to superimpose experimental values on data for meteorological stations is probably better justified on a restricted range, illustrated in Fig. 4(a) by vertical dashed lines. This is because the atmospheric dynamics is distinctly different around the equator (vanishing Coriolis force) and also around the Arctic (sea ice cover, Arctic oscillation, etc.).

The angular velocity should be also among the important variables. Experimental results for two fixed sensor locations close to the walls are shown in Fig. 4(b). There is an apparent tendency in the data (slightly decreasing ratios at higher values of Ω) loaded by rather large fluctuations. Note that the finite length of time series cannot explain the individual variability, which we tested by cutting the longest records into pieces and measuring the step number and step size ratios. The representative error bars in Fig. 4(b) were obtained in this way. The most probable reason for the variability is the nonstationary drive at the cold boundary, which is a technical limitation of our setup. As for the weather stations, it is possible that the increasing Coriolis parameter toward the pole contributes to the decreasing increment asymmetries. However, the experiments show that both the warm and cold sides have similar tendencies; thus, the overall pattern is weakly influenced by an increasing rotational speed.

Obviously, the simple experimental setup cannot model many fundamental aspects of the real atmosphere, such as the strong density stratification (compressibility), the distributed differential heating by insolation, or the latitude-dependent strength of the Coriolis effect [24]. It is not surprising, for example, that the mean temperature profiles are very different. In Fig. 5(a) we plotted the zonally averaged values of daily mean temperatures for the northern hemisphere GDCN data. The appropriate temperature profiles are quite different in the experimental tank [Fig. 5(b)] with marked thermal boundary layers of steep gradients and a dominating flat region in the middle, which is determined primarily by the boundary temperatures and affected weakly by the angular velocities in shallow layers. This behavior has

been well known since the accurate measurements by Pfeffer *et al.* [25].

As far as we could check, the asymmetry of temperature increment statistics was reported first in [2]. However, the non-Gaussian shape of histograms for fluctuation amplitudes has been noticed in many works. The deviations are usually evaluated by computing the skewness (third moment) of the empirical distribution functions, and nonzero values are often attributed to nonlinearities in the dynamics. We inspected that skewness and asymmetric increments are not correlated for our data. Recall also that surrogate time series of arbitrary skewness are fully symmetric with respect to the increments. A further issue can be to relate sampling interval and characteristic time scales of the dynamics. It is easy to see that the numerical value of the asymmetry factor depends on the sampling rate (serious undersampling results in a convergence to symmetry in any stationary time series), but the sign holds the information. This we checked by resampling both the meteorological and experimental data.

This work was supported by the Hungarian Science Foundation (OTKA) under Grants Nos. T047233 and TS044839. I.M.J thanks the János Bolyai research program for support.

[1] G. I. Barenblatt, *Scaling, Self-similarity, and Intermediate Asymptotics: Dimensional Analysis and Intermediate Asymptotics* (Cambridge University Press, Cambridge, England, 1996).
[2] I. Bartos, and I. M. Jánosi, Geophys. Res. Lett. **32**, L23820 (2005).
[3] http://www.ncdc.noaa.gov/oa/climate/research/gdcn/gdcn.html
[4] Th. Schreiber, and A. Schmitz, Physica D **142**, 346 (2000). See also http://www.mpipks-dresden. mpg. de/~tisean/
[5] D. Fultz, J. Meteorol. **6**, 17 (1949); **9**, 379 (1952).
[6] D. Fultz, R. R. Long, G. V. Owens, W. Bohan, R. Kaylor, and J. Weil, Meteorol. Monogr. **4**, 1 (1959).
[7] R. Hide, Q. J. R. Meteorol. Soc. **19**, 161 (1953); Philos. Trans. R. Soc. London, Ser. A **250**, 441 (1958).
[8] W. W. Fowlis and R. Hide, J. Atmos. Sci. **22**, 541 (1965).
[9] R. L. Pfeffer and W. W. Fowlis, J. Atmos. Sci. **25**, 361 (1968).
[10] C. B. Ketchum, J. Atmos. Sci. **29**, 665 (1972).
[11] R. Hide, P. J. Mason, and R. A. Plumb, J. Atmos. Sci. **34**, 1847 (1977).
[12] P. L. Read, M. J. Bell, D. W. Johnson, and R. M. Small, J. Fluid Mech. **238**, 599 (1992).
[13] W. G. Früh, and P. L. Read, Philos. Trans. R. Soc. London, Ser. A **355**, 101 (1997).
[14] B. Sitte and Ch. Egbers, Phys. Chem. Earth, Part B **24**, 473 (1999).
[15] Th. von Larcher and Ch. Egbers, Nonlinear Processes Geophys. **12**, 1033 (2005).
[16] R. Salmon, *Lectures on Geophysical Fluid Dynamics* (Oxford University Press, New York, 1998).
[17] R. Hide and P. J. Mason, Adv. Phys. **24**, 47 (1975).
[18] R. T. Pierrehumbert and K. L. Swanson, Annu. Rev. Fluid Mech. **27**, 419 (1995).
[19] G. K. K. Vallis, *Atmospheric and Oceanic Fluid Dynamics* (Cambridge University Press, Cambridge, England, 2006).
[20] H. Kantz and Th. Schreiber, Nonlinear Time Series Analysis, 2nd ed. (Cambridge University Press, Cambridge, England, 2004).
[21] J. Guckenheimer and G. Buzyna, Phys. Rev. Lett. **51**, 1438 (1983).
[22] T. Tél and M. Gruiz, *Chaotic Dynamics* (Cambridge University Press, Cambridge, England, 2006).
[23] *The Hadley Circulation: Present, Past and Future*, edited by H. F. Diaz and R. S. Bradley (Kluwer Academic, Dordrecht, 2005).
[24] J. Pedlosky, *Geophysical Fluid Dynamics*, 2nd ed. (Springer, New York, 2005).
[25] R. L. Pfeffer, G. Buzyna, and R. Kung, J. Atmos. Sci. **37**, 2129 (1980).